

Article

Elimination of Low-Angle Grain Boundary Networks in FeCrAl Alloys with the Electron Wind Force at a Low Temperature

Md Hafijur Rahman ¹, Sarah Todaro ¹, Luke Warner ¹, Daudi Waryoba ²  and Aman Haque ^{1,*}

¹ Department of Mechanical Engineering, University Park, The Pennsylvania State University, State College, PA 16803, USA; mrx5923@psu.edu (M.H.R.); set5410@psu.edu (S.T.); lfw5312@psu.edu (L.W.)

² Engineering, Applied Materials, Penn State University, 1 College Place, DuBois, PA 15801, USA; drw29@psu.edu

* Correspondence: mah37@psu.edu

Abstract: Low-angle grain boundaries (LAGBs) accommodate residual stress through the rearrangement and accumulation of dislocations during cold rolling. This study presents an electron wind force-based annealing approach to recover cold-rolling induced residual stress in FeCrAl alloy below 100 °C in 1 min. This is significantly lower than conventional thermal annealing, which typically requires temperatures around 750 °C for about 1.5 h. A key feature of our approach is the athermal electron wind force effect, which promotes dislocation movement and stress relief at significantly lower temperatures. The electron backscattered diffraction (EBSD) analysis reveals that the concentration of low-angle grain boundaries (LAGBs) is reduced from 82.4% in the cold-rolled state to a mere 47.5% following electropulsing. This level of defect recovery even surpasses the pristine material's initial state, which exhibited 54.8% LAGBs. This reduction in LAGB concentration was complemented by kernel average misorientation (KAM) maps and X-ray diffraction (XRD) Full Width at Half Maximum (FWHM) measurements, which further validated the microstructural enhancements. Nanoindentation tests revealed a slight increase in hardness despite the reduction in dislocation density, suggesting a balance between grain boundary refinement and dislocation dynamics. This proposed low-temperature technique, driven by athermal electron wind forces, presents a promising avenue for residual stress mitigation while minimizing undesirable thermal effects, paving the way for advancements in various material processing applications.



Citation: Rahman, M.H.; Todaro, S.; Warner, L.; Waryoba, D.; Haque, A. Elimination of Low-Angle Grain Boundary Networks in FeCrAl Alloys with the Electron Wind Force at a Low Temperature. *Metals* **2024**, *14*, 331. <https://doi.org/10.3390/met14030331>

Academic Editors: Ahmed Al-Kattan and Catalin Constantinescu

Received: 22 February 2024

Revised: 11 March 2024

Accepted: 12 March 2024

Published: 14 March 2024



Copyright: © 2024 by the authors. Licensee MDPI, Basel, Switzerland. This article is an open access article distributed under the terms and conditions of the Creative Commons Attribution (CC BY) license (<https://creativecommons.org/licenses/by/4.0/>).

1. Introduction

FeCrAl (Iron-Chromium-Aluminum) alloys hold significant importance due to their exceptional oxidation and corrosion resistance at elevated temperatures, alongside favorable mechanical properties and stability under aggressive conditions [1,2]. These advantages make FeCrAl alloys the preferred materials for a wide range of high-temperature applications, including heating elements, automotive exhaust systems, industrial furnaces, and cladding material in nuclear reactors [3–5]. Despite their robust performance, Sun et al. [6] observed that commercial FeCrAl alloys often possess residual strain stemming from the fabrication process, which they suggest can be mitigated through annealing treatments to enhance material reliability and longevity. Moreover, certain applications may require the cold rolling of FeCrAl alloys to meet specific mechanical strength, dimensional accuracy, or surface finish criteria [7]. Cold rolling, a pivotal process in materials engineering, is utilized to enhance the mechanical properties of metals through plastic deformation. It is well-documented that cold rolling not only contributes to hardening by generating dislocations within the material's structure [8,9] but also inherently introduces residual stresses [10,11]. While cold rolling is instrumental in improving strength and hardness,

the additional residual stresses it introduces can complicate the material's microstructural integrity. Consequently, it is imperative that residual stress, whether arising from the fabrication process or induced by cold rolling, needs to be alleviated to maintain the FeCrAl alloy's desired properties and performance.

The induced residual stresses are usually accommodated within the grains by low-angle grain boundaries (LAGBs) [12]. These LAGBs, characterized by slight misorientations between adjacent crystalline areas, have a direct correlation with the extent of residual stress within a material [13]. To mitigate these induced stresses, conventional methods such as thermal annealing, cryogenic treatment, and chemical treatments are commonly utilized [14–18]. However, these traditional techniques often present challenges, including high energy consumption, prolonged processing times, and the risk of inducing additional microstructural changes, such as unwanted phase transformations [19,20]. Consequently, the quest for alternative approaches that can efficiently and effectively reduce residual stress without these drawbacks is ongoing.

Electropulsing treatment (EPT), which applies short, high-intensity electrical pulses, has emerged as a promising technique in this context, offering the potential to modify the microstructure and alleviate residual stresses of materials and alloys [21–25]. The application of electropulsing to materials induces two distinct types of effects: athermal and thermal [26–28]. The electron wind force is a non-thermal force exerted by the conduction electrons, which are driven through the material by the electric field. As these electrons collide with the defects, they lose momentum. The defects experience a mechanical force due to the momentum transfer, which mobilizes them [27,29]. On the other hand, the thermal effect, which arises from Joule heating, is the heat generated by the passage of current through the resistive material, leading to an increase in the material's temperature [26,27]. The fundamental mechanism for reducing residual stress in alloys is currently debated. Some researchers suggest that electron wind force plays a key role, while others believe Joule heating is more influential [21–25]. For example, Zhang et al. [23] argue that the key to residual stress reduction lies not in Joule heating but in the action of drift electrons, which purportedly exert an additional force aiding dislocation movement. Conversely, Pan et al. [21] contend that the primary influence on dislocation dynamics stems from Joule heating, with the electron drag force playing a negligible role. However, in most cases, it is believed that a synergistic effect of both Joule heating and EWF is responsible for residual stress mitigation, suggesting a complex interplay at the microstructural level. Interestingly, Huang et al. [30] reported a 20% increase in residual stress in 16 Mn steel plates post-electropulsing, raising questions about the method's reliability and indicating the need for more research to understand its impact and potential for industrial use. Moreover, most of the existing research on the elimination of residual stress through electropulsing treatment (EPT) has been concentrated on steel, with little to no focus on its application to FeCrAl alloys for residual stress annealing. Electropulsing has conventionally been applied with a significant increase in temperature by Joule heating [27,31,32].

This study proposes an innovative approach to anneal the residual stress in FeCrAl alloy induced from cold rolling through EPT, emphasizing the athermal electron wind force (EWF) effect associated with electropulsing. While thermal and athermal effects in electropulsing treatments are distinct, they are not mutually exclusive. Achieving a high electron wind force (EWF), essential for promoting dislocation movement and reducing residual stress, necessitates an increase in current density [33,34]. However, this increase in current density invariably enhances Joule heating and thus increases the processing temperature [35], making it challenging to isolate the effects of the thermal and athermal components of electropulsing. In this study, we address this challenge by pulsed current supply, distinct from the constant elevated temperatures typically reported [22]. This still gives rise to temperature spikes, but the very low-duty cycle ensures a minimal rise in average temperature. By employing low frequency and narrow pulse widths, we successfully minimize thermal effects, maintaining the average temperature below 100 °C, even at an elevated current density of $3.35 \times 10^5 \frac{A}{cm^2}$. The use of short pulse width and low

frequency provides sufficient time for heat to dissipate before the next pulse, minimizing the risk of excessive Joule heating [25,36,37]. This approach offers a more controlled exploration of how electropulsing can be optimized to exploit the beneficial aspects of EWF while mitigating the potential drawbacks of excessive Joule heating, thereby advancing our ability to distinguish between the thermal and athermal contributions to stress mitigation in electropulsing treatments.

Utilizing a comprehensive analytical approach, we examine low-angle grain boundary (LAGB) concentrations, and Kernel Average Misorientation (KAM) maps through electron backscattered diffraction (EBSD) analysis. Additionally, we measure the Full Width at Half Maximum (FWHM) using X-ray diffraction (XRD) to complement the microstructural changes observed in EBSD analysis and conduct nanoindentation tests to evaluate the mechanical properties. This detailed examination aims to underscore the potential of low-temperature EPT as an effective method for enhancing the properties of FeCrAl alloys by mitigating their residual stresses.

2. Materials and Methods

In this study, we explored the potential of electropulsing as an alternative method to traditional thermal annealing for the mitigation of residual stress in a FeCrAl alloy (Fe-73%, Cr-21.3%, Al-5.7%). The process commenced with the intentional introduction of residual stress by cold rolling the alloy, altering its dimensions from $10.5 \times 2.6 \times 0.22 \text{ mm}^3$ to $11.5 \times 3.26 \times 0.16 \text{ mm}^3$ (~27% reduction of thickness). Subsequently, electropulsing was administered in two distinct phases: initially at a moderate temperature of $\sim 30^\circ\text{C}$, followed by a more intensive stage with high current density allowing the temperature to escalate to a maximum of 125°C . This procedure was facilitated by a programmable DC power supply (model: Magna-power, Flemington, NJ, USA, SL600-2.5/UI) connected to a current pulse generator (Eagle Harbor, Seattle, WA, USA, IPM-16P-2003), with a thermal microscope (Optis, Portsmouth, NH, USA, PI 640) deployed to accurately record the temperature dynamics throughout the processing period, the results of which are depicted in Figure 1. The figure illustrates the temperature profile of a sample subjected to electropulsing over a period of 60 s. The cyclic pattern suggests that the sample has sufficient time to dissipate heat between pulses, resulting in a temperature profile that repeatedly rises sharply and then falls back as the heat is dissipated before the next pulse begins. The electropulsing parameters employed are presented in Table 1.

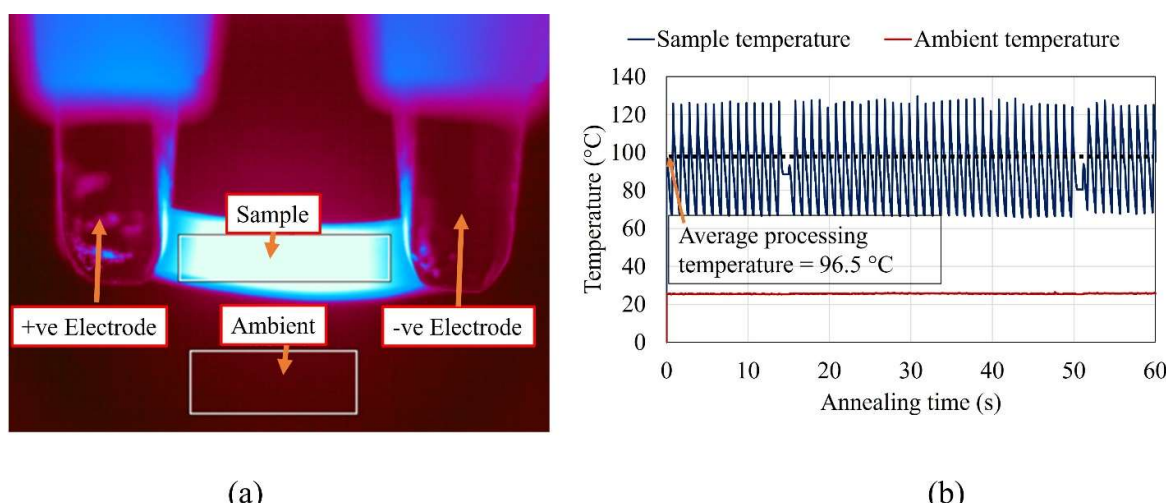


Figure 1. (a) Thermograph image and (b) temperature profile of sample and ambient for 1 min of annealing period with a current density of $3307.7 \frac{\text{A}}{\text{mm}^2}$.

Table 1. Electron wind force annealing parameters and corresponding processing temperatures.

Frequency (Hz)	Pulse Width (μs)	Processing Time (s)	Current Density ($\frac{A}{mm^2}$)	Average Temperature during Annealing (°C)
2	40	60	235.15	25
2	40	60	1230.85	28.5
2	40	60	1805.31	50
2	40	60	2215.38	65
2	40	60	2666.67	85
2	40	60	3307.70	96.5

The selection of processing parameters, such as current density, pulse width, and frequency, was made strategically, drawing upon our extensive experience with similar materials, as detailed in our prior work [36]. The pulse width was deliberately kept short at 40 microseconds, ensuring the sample receives a concise energy input, allowing ample time between pulses for heat dissipation and thus maintaining EWF as the dominant influencing factor. Similarly, the frequency was set to a low 2 Hz to prevent excessive heating that could shift the balance towards thermal effects, undermining the intended athermal mechanism of action. It is to be noted that the electron wind force from the sharp pulses transfers the shock wave energy to the defects. Since defect motion is irreversible and depends on the input energy level, our technique needs only a few cycles (or seconds) of pulsing. Prolonged application of pulsing does not improve unless the energy (such as current density) is increased. We pulsed the sample for 60 s just to make sure that a steady state had been reached. This methodology reflects a careful balance between optimizing energy transfer to defects and ensuring minimal thermal influence, underpinning the effectiveness of our EPT technique.

The electron backscatter diffraction (EBSD) and X-ray diffraction (XRD) analyses were conducted to provide a comprehensive characterization of the sample's microstructure at each stage of the experiment—initial (pristine), after cold rolling, following the first electropulsing phase, and after the second electropulsing phase. Prior to conducting electron backscatter diffraction (EBSD) analysis, the sample underwent extensive surface preparation to render the surface suitable for microscopy. This involved a thorough polishing regimen using a rotary tool and a series of diamond compounds ranging from 3000 to 120,000 grit, followed by ion milling at 4.5 kV and 1.5 Å for 90 min to achieve a suitably refined surface. EBSD analysis was then performed using a VERIOS G4 UC Scanning Electron Microscope (Thermoscientific, Hillsboro, OR, USA), set to a beam current of 3.2 nA, an accelerating voltage of 20 KV, and a step size of 0.3 μm, utilizing the Aztec software suite version 6.2 for data collection. The acquired EBSD data were post-processed and thoroughly analyzed using the dedicated Aztec Crystal software suite version 5.1 [38].

The XRD measurements were carried out with a Malvern Panalytical Empyrean® instrument, equipped with a cobalt line-focus X-ray tube (wavelength = 1.7890 Å) and optimized for comprehensive sample area irradiation, adhering to specific settings for divergence slit of $(\frac{1}{16})^\circ$, mask of 2 mm, soler slit of 0.04 rad, and anti-scatter slit of $(\frac{1}{4})^\circ$. Finally, to evaluate the impact of the electropulsing treatments on the mechanical properties, nanoindentation tests were conducted using a Bruker Hysitron TI-980 instrument. These experiments aimed to measure changes in hardness and reduced modulus resulting from the treatments.

3. Results and Discussion

3.1. Microstructure and Grain Boundaries (GBs) Evolution

The microstructural integrity and mechanical properties of FeCrAl alloys are profoundly influenced by the manufacturing processes they undergo. In this study, we have intentionally utilized cold rolling to increase the defect density within a FeCrAl alloy, setting the stage for investigating the efficacy of electropulsing as an innovative annealing

alternative. The y -axis Inverse Pole Figure (IPF) maps in Figure 2 display the various microstructural states of the alloy from its pristine condition, through the intentional defect introduction by cold rolling, to the modifications after electropulsing at controlled average temperatures of 28.5 °C and 96.5 °C. The intentional induction of defects through cold rolling in our FeCrAl alloy led to a marked increase in the concentration of low-angle grain boundaries (LAGBs) from 54.8% in its pristine state to 82.4%, indicative of the high residual strain imposed on the material (see Figure 3). These LAGBs are characterized by misorientations between 2° and 10°. Such an increase aligns with the understanding that cold deformation intensifies the entanglement of dislocations within the crystal lattice, which, in turn, impedes further dislocation movement and contributes to residual stress accumulation [8,9].

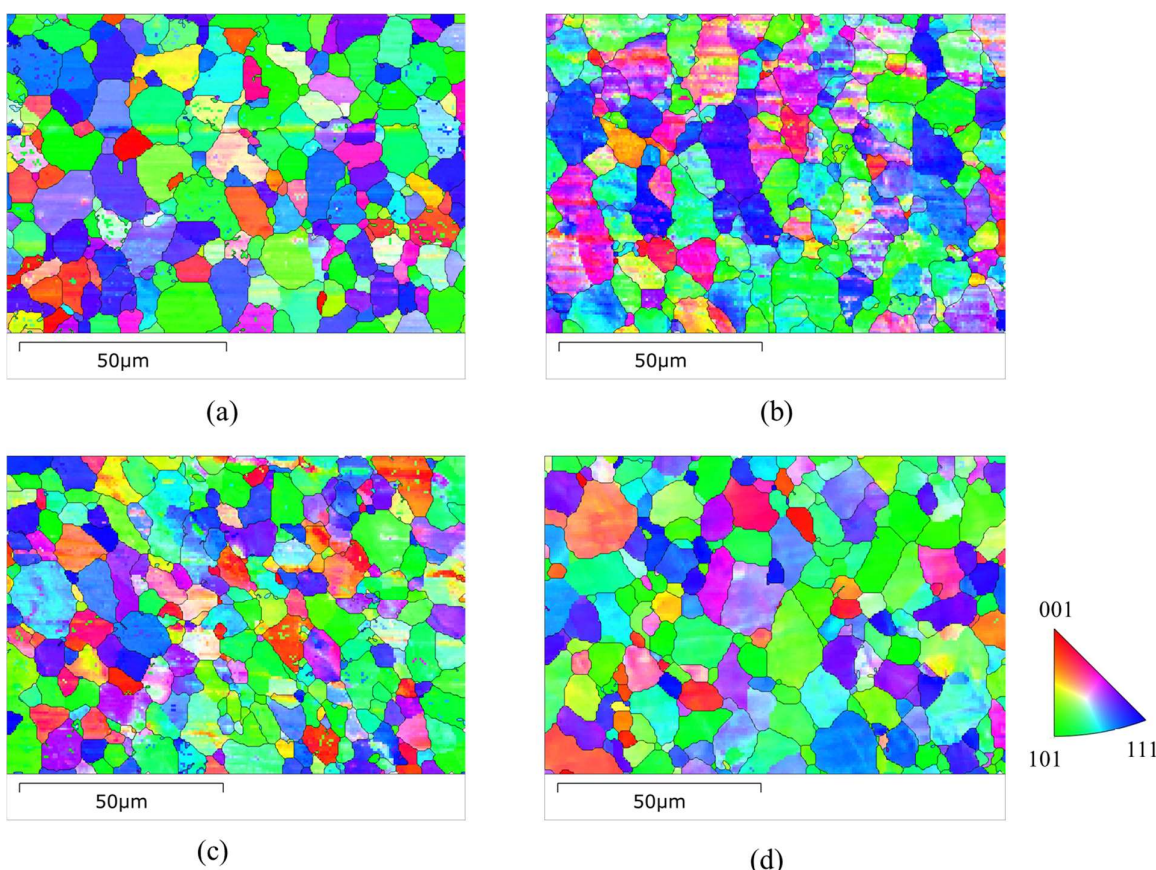


Figure 2. Microstructure of sample (yIPF maps) in various conditions: (a) pristine, (b) cold rolled to ~27% reduction of thickness, (c) pulsed at 28.5 °C, and (d) pulsed at 96.5 °C.

The subsequent application of the electron wind force at 28.5 °C yielded a reduction in LAGB concentration to 70.5%, suggesting the onset of dislocation disentanglement. Drawing on analogous discussions from existing literature, such as the study on titanium alloys [29], we consider a similar mechanistic interpretation for our observations. The entangled dislocations generated through cold deformation, which serve as impediments to the mobility of dislocations, are conjectured to be swiftly disrupted under the influence of the electron wind force. This athermal stimulus is believed to cause dislocations to migrate and pile up at grain boundaries, potentially forming dislocation walls that transform LAGBs into high-angle grain boundaries, thus facilitating the process of recrystallization and stress reduction in the alloy [29]. The influence of the electron wind force is dependent on the current density during electropulsing. A higher current density means a larger number of electrons are flowing through the material, which can increase the momentum transfer to the dislocations and thus enhance the electron wind force. As a result, the rate of dislocation

movement can increase, leading to more effective disentanglement and migration. However, this high current density can lead to an increase in the material's temperature during the processing. It is well-established that the peak temperature increment induced by a singular electropulse is quantitatively related to the current density.

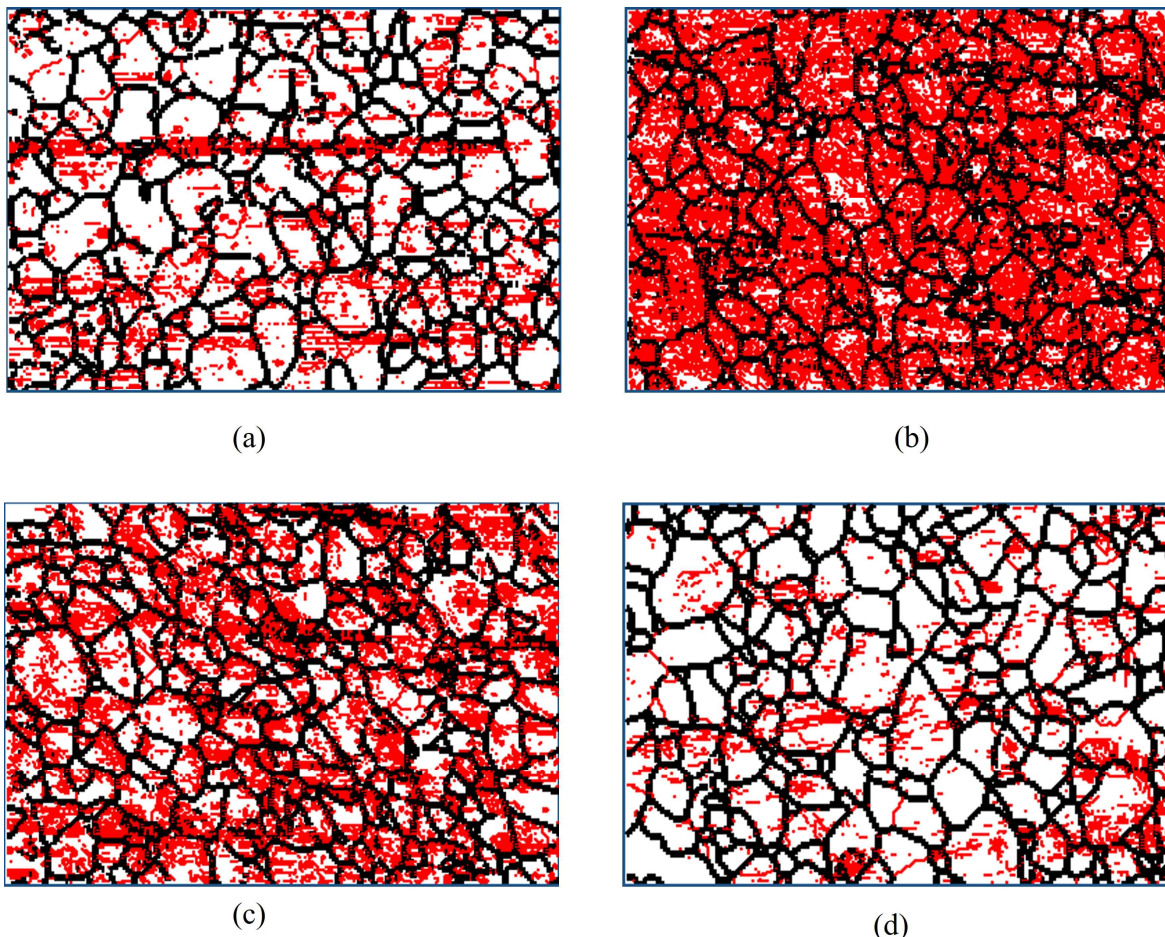


Figure 3. Grain boundaries for various conditions (a) pristine, (b) cold rolled to ~27% reduction of thickness, (c) pulsed at 28.5 °C, and (d) pulsed at 96.5 °C; Red color indicates low angle grain boundaries-LAGBs ($2^\circ \leq \theta \leq 10^\circ$).

As detailed in [39], this temperature rise, denoted as ΔT_m , is governed by the following relationship:

$$\Delta T_m = \frac{t_c \rho j_m^2}{2C_p D} \quad (1)$$

where t_c is the pulse width, ρ is the resistivity of the materials, C_p is the specific heat, D is the density of the materials, and j_m is the current density amplitude of the applied electropulse. Although the thermal effect causes changes in microstructure and properties through mechanisms like recrystallization, and grain growth, in this study, we focused on the athermal effect. By using low pulse widths and low frequencies, the Joule heating is restricted, thus limiting the temperature rise (see Figure 1). The dislocation disentanglement within our FeCrAl alloy commenced at a current density of 1230.85 A/mm². To advance this disentanglement process, the current density was elevated to 3307.7 A/mm² with a processing temperature of an average of 96.5 °C. For this current density of 3307.7 A/mm², theoretical calculations using Equation (1) suggested a maximum temperature rise of 92.5 °C, which, with an ambient starting temperature of 25.5 °C, projected a maximum processing temperature of 118 °C. Our observations revealed a slightly higher maximum

temperature of 125 °C during the treatment, with an average temperature of 96.5 °C throughout the process. This slight discrepancy between the expected and observed temperatures can be attributed to several factors. Notably, the cold rolling process likely introduced localized thin sections within the material, leading to uneven current densities during electropulsing. These localized areas of increased current density would experience enhanced Joule heating, generating hot spots that elevate the temperature beyond the calculated value. However, this increased current density exerts a stronger electron wind force, which reduced the concentration of low-angle grain boundaries (LAGBs) to 47.5%, a figure that notably falls below the initial pristine state of the alloy. This substantial decrease in LAGB concentration post-EP treatments is indicative of the process's effectiveness in not only reversing the cold rolling effects but also enhancing the microstructure. It is critical to highlight that typically, such a high current density during electropulsing would result in a material temperature of around 600 °C [31]. However, by employing controlled electropulsing parameters, we were able to limit the average processing temperature to 96.5 °C, thereby minimizing the thermal effects while still capitalizing on the benefits of the electron wind force to modify the microstructure.

The significance of HAGBs in reducing the dislocation density and recrystallization during the electric pulse processing is also imminent. As we discussed earlier, the electron wind force (EWF) acts to disentangle and mobilize the LAGBs and thus enhance their interaction with existing HAGBs. As these mobile LAGBs encounter HAGBs, they begin to accumulate and undergo a transformation into HAGBs themselves. This kind of transformation leads to reduced density of dislocations to the material. Such transformation of LAGBs to HAGBs is reported in [40,41]. On the other hand, HAGBs emerge as potential centers for recrystallization. When low-angle grain boundaries (LAGBs), mobilized by the EWF, approach HAGBs, the subsequent interaction leads to the accumulation of subgrains around these high-energy boundaries. This phenomenon plays a crucial role in the microstructural evolution process, as the accumulation and consolidation of subgrains near HAGBs can effectively divide parent grains, resulting in a finer grain structure. The division and refinement of grains contribute to a smaller mean grain size across the treated alloy.

A comprehensive grain size analysis is shown in Figure 4, revealing the microstructural changes under different conditions—Pristine, Rolled, and Pulsed at 96.5 °C. Initially, the rolling process altered the grain size distribution, notably decreasing the frequency of smaller grains while increasing that of larger grains, culminating in an overall mean grain size increase from 6.0 µm in the pristine condition to 7.2 µm post-rolling. This observation aligns with the expected effects of mechanical deformation, where grain elongation and the merger of smaller grains contribute to an increased mean grain size. Conversely, after the application of electropulsing treatment, a notable shift in the grain size distribution was observed. Specifically, there was an increase in the frequency of smaller grains, while the distribution of larger grains remained relatively unchanged. This shift towards smaller grain sizes is indicative of the material undergoing microstructural refinement induced by the electron wind force. Such grain refinement, facilitated by electric current assistance, as observed in our study, aligns with the findings reported in [42–44]. As a result, the mean grain size was reduced to 6.5 µm, underscoring the potential of electric processing to refine the grain structure and partially reverse the coarsening effects introduced by cold rolling.

3.2. Microstructural Analysis through Misorientation Maps

The microstructural modifications induced by cold rolling and subsequent electropulsing treatments are quantitatively depicted through Kernel Average Misorientation (KAM) maps (Figure 5) and the distribution of disorientation angles (Figure 6). In our KAM analysis, we employed a kernel size of 3 × 3, averaging misorientation over each pixel and its eight immediate neighbors, to accurately capture local texture variations indicative of stress states. Following the cold rolling process, we observed an increase in the Kernel Average Misorientation (KAM). The increase in KAM values post-cold rolling is indicative of elevated internal strain, reflecting the introduced dislocation density and the resultant

residual stress within the material [45]. Li et al. [46] demonstrated that deformed grains exhibit increased KAM values due to elevated dislocation densities. This increase in KAM is further substantiated by the disorientation angle distribution, where the rolled state in Figure 6 exhibits an intense peak, indicating a densification of dislocations. Moreover, the observation is consistent with the well-established notion that mechanical deformation, such as cold rolling, significantly raises the residual stress of a material [47]. Although the values of residual stresses obtained from EBSD Kernel Average Misorientation (KAM) measurements are not absolute, Terner et al. [48] have established a correlation between KAM values and the level of residual stress. It is observed that higher KAM values correspond to elevated levels of residual stress. Therefore, our observation of increased KAM after cold rolling is consistent with an increase in residual stress, aligning with the established expectations. Subsequent electropulsing treatments resulted in a gradual decrease in KAM values as well as the peak intensity of the disorientation angle. The first pulse at 28.5 °C initiated the reduction of strain, indicating the start of microstructural recovery. The effect was more pronounced after the final pulse at the higher current density, where the KAM values and the distribution of disorientation angle approached those of the pristine alloy. This substantial decrease in KAM points to a decrease in dislocation density and, by extension, suggests that electropulsing, particularly at elevated current densities, is instrumental in effectively reducing the residual stresses and thus restoring the alloy's microstructure.

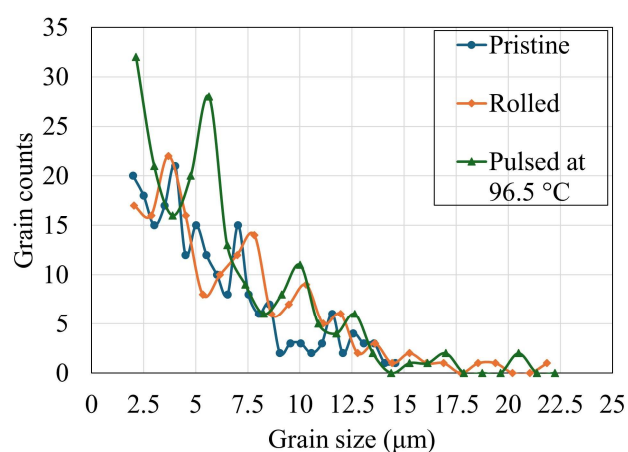


Figure 4. Grain size distribution for various conditions.

3.3. Microstructural Characterization through X-ray Diffraction (XRD) Analysis

The X-ray diffraction (XRD) analysis further complements our understanding of the microstructural evolution of the FeCrAl alloy through various stages of the treatment. Initially, the XRD pattern of the pristine FeCrAl alloy exhibited three distinct peaks labeled A, B, and C (Figure 7). After subjecting the alloy to cold rolling, an increase in the Full Width at Half Maximum (FWHM) was noted for all three peaks: Peak A increased by 48.76%, Peak B by 58.1%, and Peak C by 60.27%. These enlargements in FWHM are indicative of an increase in defect density, dislocation, and residual stress within the material [49,50]. Notably, there was no evidence of secondary phase formation due to cold rolling. Following the electropulsing treatment at 96.5 °C, the FWHM of Peak A decreased by approximately 48.91% and Peak C by approximately 40.6%, approaching the sharpness of the pristine state, which signifies a substantial recovery from the defects and residual stress introduced by cold rolling. However, the FWHM of peak B, after electropulsing, displayed a reduction of 12.64%, which, despite a decrease from the rolled condition, did not return as close to the pristine value. This behavior implies that the lattice planes associated with peak B may have a different response to the electropulsing treatment compared to those of peaks A and C.

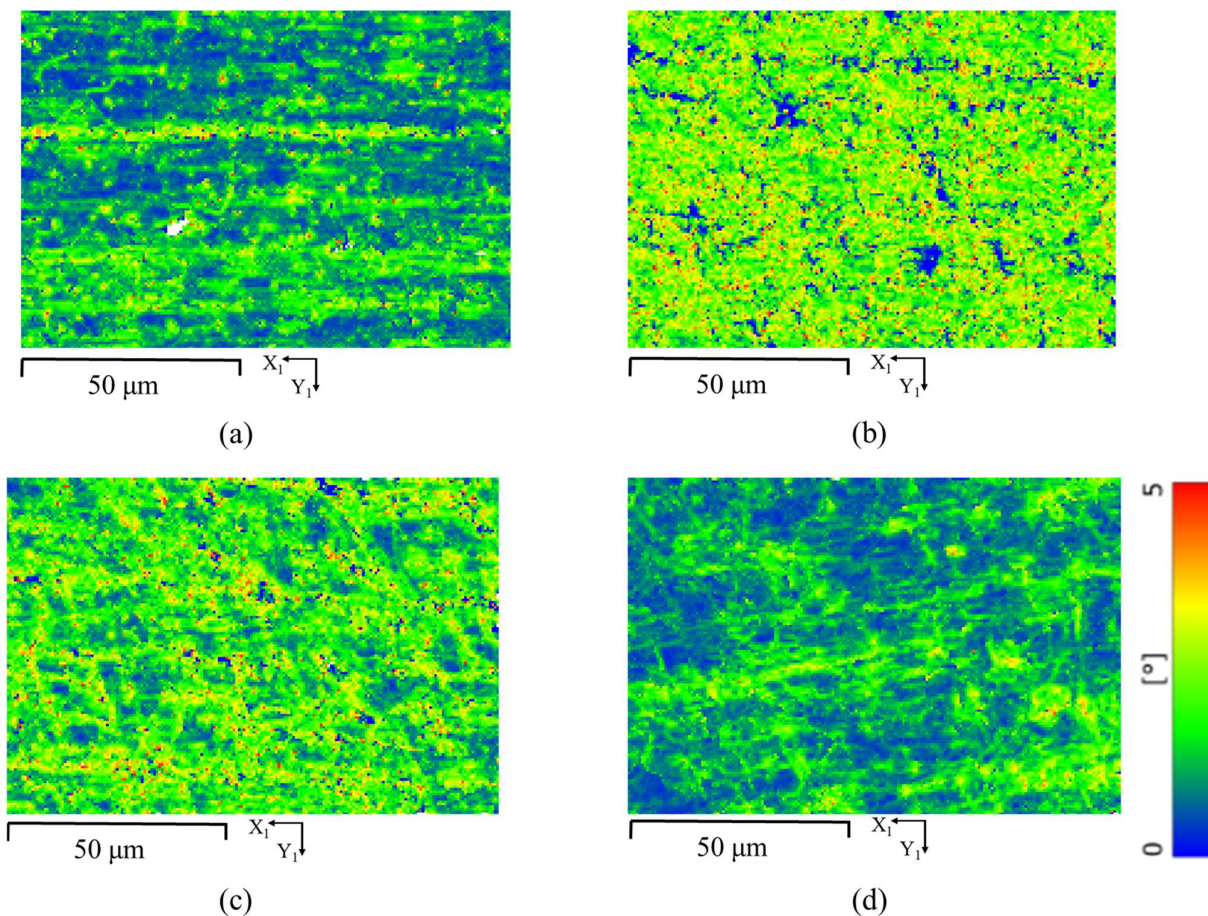


Figure 5. Kernel average misorientation (KAM) maps for various conditions: (a) pristine, (b) cold rolled to ~27% reduction of thickness, (c) pulsed at 28.5 °C, and (d) pulsed at 96.5 °C.

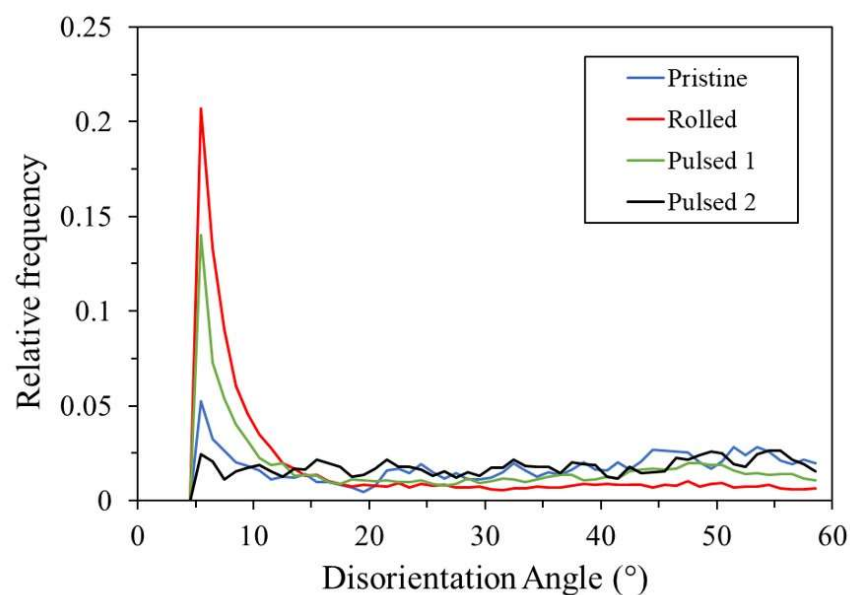


Figure 6. Disorientation angle distribution for pristine, cold rolled, and electropulsed samples. Pulsed 1 and Pulsed 2 represent pulsing at 28.5 °C and 96.5 °C, respectively.

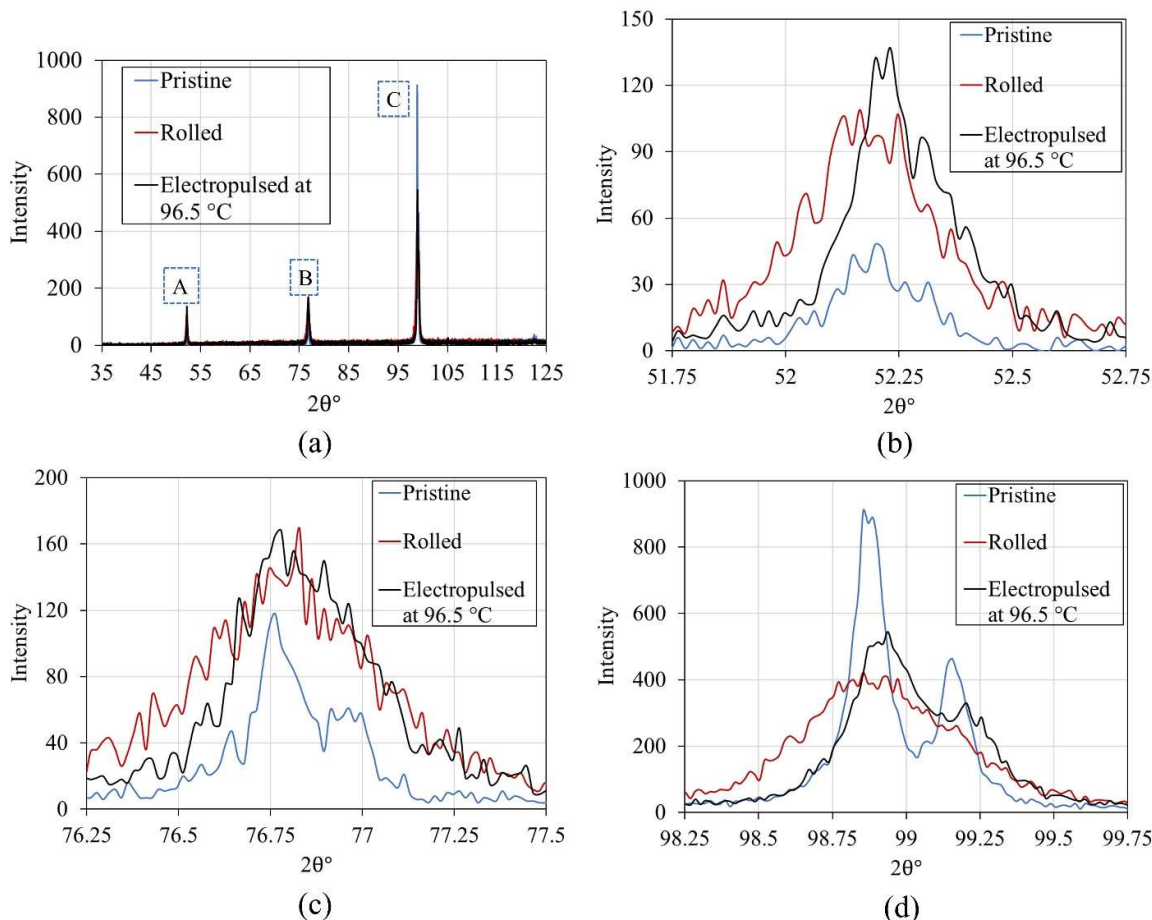


Figure 7. X-ray diffraction pattern of FeCrAl alloys for pristine, cold rolled, and electropulsed conditions; (a) pattern for $35^{\circ} \leq 2\theta^{\circ} \leq 125^{\circ}$ with three distinct peaks denoted as peak A, peak B, and peak C; (b–d) are the zoomed-in sections of peak A, peak B, and peak C, respectively.

These changes in FWHM are quantitatively detailed in Table 2, providing a clear view of the material's response to the electropulsing treatment. These precise FWHM measurements from the XRD peaks reinforce the findings from the microstructural analysis made via KAM maps and disorientation angle distributions, providing a holistic picture of the stress-relief and recrystallization processes occurring within the FeCrAl alloy because of electropulsing, albeit with varying degrees of effectiveness across different crystallographic orientations.

Table 2. Full width at half max (FWHM) along with % change of three peaks for various conditions.

FWHM	Pristine	Rolled	Pulsed at $96.5\text{ }^{\circ}\text{C}$
Peak A	0.2151°	0.320° (+48.76%)	0.215° (-48.91%)
Peak B	0.284°	0.449° (+58.1%)	0.413° (-12.64%)
Peak C	0.36°	0.577° (+60.27%)	0.431° (-40.6%)

3.4. Texture Evolution and Grain Rotation during Electropulsing

Grain rotation, a common phenomenon associated with electropulsing [36,51], was evident in our study. In our analysis of the texture evolution through pole figure examinations in Figure 8, we noted a more prominent change in the HCP phase compared to the BCC phase during electropulsing. For the BCC phase in its pristine state, a pronounced $\langle 111 \rangle$ texture is visible, with the plane oriented parallel to the Z-axis, highlighted by an intense red coloration. Upon rolling, this distinct red intensity faded away slightly, suggesting a reduction in the $\langle 111 \rangle$ texture density. However, after the final electropulsing treatment,

the $\langle 111 \rangle$ pole intensity is restored, indicating a reorientation or recovery of the grains back toward the original $\langle 111 \rangle$ texture. In the case of the HCP phase, the pristine condition displays a strong pole near the $\langle 10\bar{1}0 \rangle$ plane, which is markedly reduced after rolling. Concurrently, the rolling process introduces a visible pole near the $\langle 0001 \rangle$ plane, shifting the texture emphasis away from the $\langle 10\bar{1}0 \rangle$ orientation. After electropulsing, the pole figure evolves further: the $\langle 0001 \rangle$ plane's intensity becomes more pronounced, and there is a slight resurgence of the $\langle 10\bar{1}0 \rangle$ plane's visibility, suggesting a partial reversion towards the initial texture.

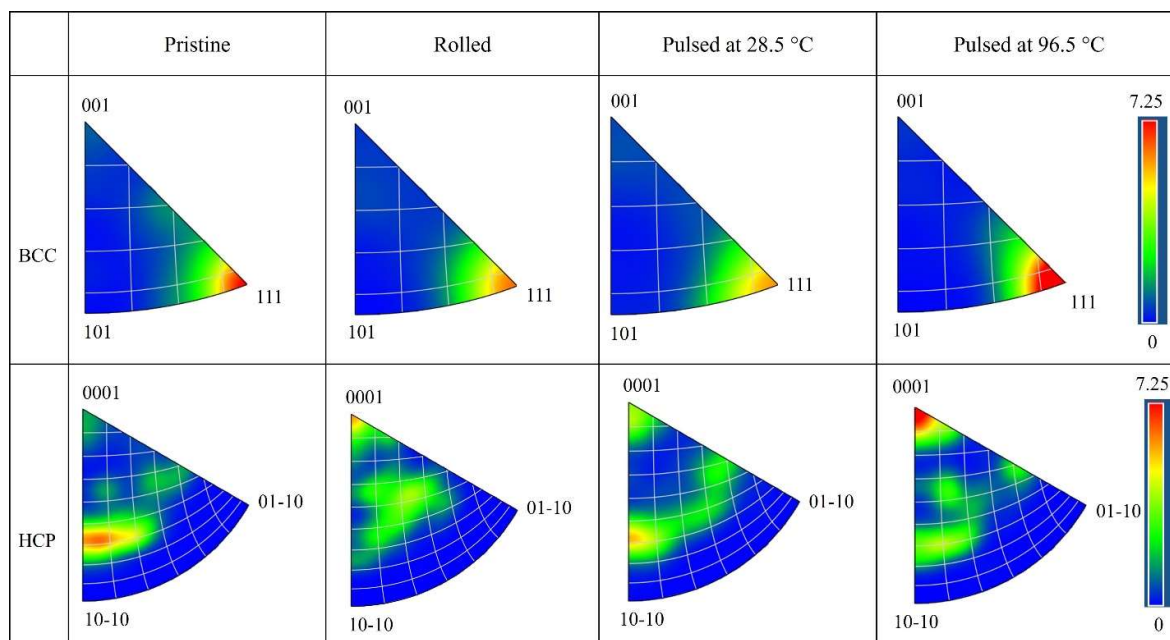


Figure 8. Pole figures with respect to the Z-axis (normal to sample surface) of the bcc and hcp phases for various conditions.

3.5. Evaluation of Mechanical Properties through Nanoindentation Testing

In the final phase of our study, the nanoindentation tests were performed at nine separate locations on the sample for the pristine, rolled, and pulsed conditions, as illustrated in Figure 9, to examine the mechanical properties of the FeCrAl alloy under different processing conditions. The obtained average values for hardness and reduced modulus for each state are provided in Table 3. After cold rolling, both the hardness and the reduced modulus of the alloy were observed to increase by 15.66% and 14.04%, respectively. The increase in hardness due to cold rolling can be attributed to the work hardening effect, where the introduction of a high density of dislocations impedes the movement of other dislocations, thereby increasing the material's resistance to plastic deformation.

Table 3. Average hardness and reduced modulus (along with percentage changes) for various conditions obtained from nanoindentation.

Conditions	Hardness (GPa)	Reduced Modulus (GPa)
Pristine	4.47 ± 0.22	160.4 ± 3.52
Rolled	5.17 ± 0.18 (+15.66%)	182.9 ± 3.96 (+14.04%)
Pulsed	5.35 ± 0.19 (+3.5%)	161.4 ± 3.32 (-11.8%)

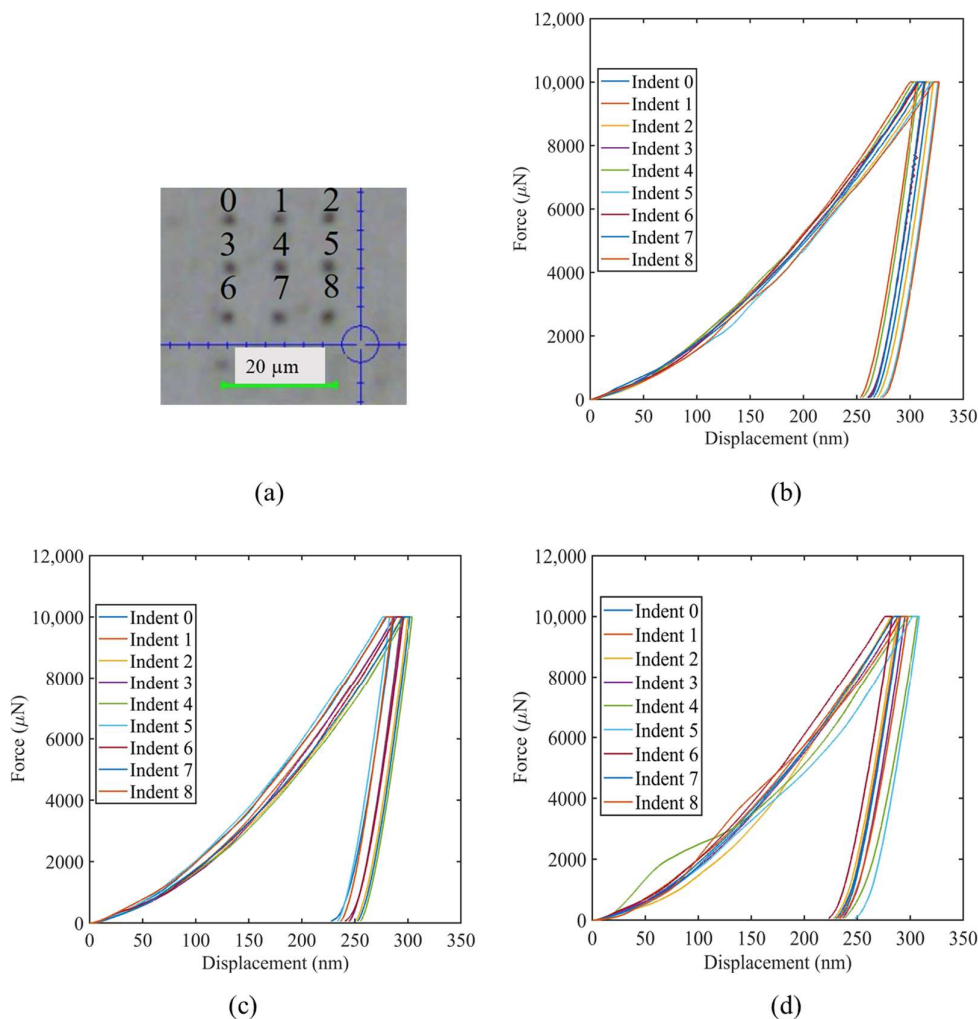


Figure 9. (a) Displays the nine indent points and load-displacement curves for (b) pristine, (c) cold rolled to ~27% reduction of thickness, and (d) pulsed at 96.5 °C obtained by nanoindentation.

Moreover, Zhao et al. [52] discussed that, during nanoindentation, an elevated reduced modulus is typically observed at higher penetration depths, where a ‘forest’ of dislocation entanglement forms. Analogously, cold rolling introduces a high density of dislocations into the FeCrAl alloy system, akin to dislocation pinning hardening. Consequently, the presence of these pre-existing dislocations contributes to a higher reduced modulus.

Upon electropulsing, the anticipated reduction in hardness due to decreased dislocation density was not straightforwardly reflected in our observations. While electropulsing is typically expected to lower the hardness by reducing the dislocations introduced by cold rolling, our measurements indicated a slight increase in hardness by 3.5%, a value that falls within the margin of experimental error. This suggests that contrary to expectations, electropulsing either slightly increases hardness or maintains it at a level comparable to the post-rolling state. This paradoxical outcome merits further explanation. Notably, after electropulsing, we observed a slight reduction in mean grain size (from 7.2 μm post-rolling to 6.5 μm following the pulsing treatment), a factor that, according to the Hall-Petch relationship, should inherently increase the hardness. Conversely, the observed decrease in dislocation density should theoretically lead to a decrease in hardness, presenting two opposing influences. We hypothesize that these conflicting effects—grain size refinement and dislocation density reduction—may neutralize each other’s impact on hardness, resulting in an overall hardness that is nearly unchanged following electropulsing. On the other hand, the reduced modulus was seen to revert nearly to its pristine condition post-electropulsing. This suggests that while the material retains the hardness imparted by the cold work due

to the aforementioned mechanisms, the stiffness of the material, as it relates to elastic deformation, returns to close to its original state due to the relief of residual stresses and the restoration of the microstructure toward its pre-deformed lattice arrangement.

4. Conclusions

This study successfully demonstrates the potential of low-temperature annealing, utilizing electron wind force (EWF), as an innovative and efficient technique for mitigating residual stresses and defects induced by cold rolling in FeCrAl alloys. Key findings include the following:

- A significant reduction in low-angle grain boundary (LAGB) concentration from 82.4% in the cold-rolled state to 47.5% post-electropulsing, surpassing the initial condition's 54.8%, thereby illustrating the effectiveness of EWF in microstructural refinement.
- The application of electropulsing led to notable texture changes, with the hcp phase showing more significant texture evolution than the bcc phase, indicating a pronounced impact on microstructural orientation.
- XRD analysis confirmed improvements in the FWHM for peaks A and C post-electropulsing, signifying a decrease in defect density and residual stress, whereas the less pronounced recovery for peak B suggests that the effectiveness of EWF annealing may be lattice-plane dependent.
- Nanoindentation tests showed a slight increase in hardness by 3.5%, and the reduced modulus approached near-pristine levels post-electropulsing, suggesting a balance between grain boundary strengthening and dislocation density reduction.

By employing a unique combination of low frequency and short pulse width, our method not only minimized Joule heating but also established a low-temperature processing regime, effectively enhancing the mechanical and microstructural properties of the treated FeCrAl alloy.

Author Contributions: Conceptualization, M.H.R. and A.H.; methodology, M.H.R., S.T. and L.W.; software, M.H.R. and D.W.; formal analysis, M.H.R.; writing—original draft preparation, M.H.R.; writing—review and editing, A.H., D.W., S.T. and L.W.; supervision, A.H. and D.W.; funding acquisition, A.H. All authors have read and agreed to the published version of the manuscript.

Funding: This research was funded by the US Army Research Office through award #W911NF-23-1-0359. The authors also acknowledge partial support from the Division of Materials Research, Metal & Metallic Nanostructure Program through award #2103928. Any opinions, findings, and conclusions or recommendations expressed in this material are those of the author and do not necessarily reflect the views of the sponsors.

Data Availability Statement: The raw data supporting the conclusions of this article will be made available by the authors on request.

Conflicts of Interest: The authors declare no conflicts of interest.

References

1. Klöwer, J. High Temperature Corrosion Behaviour of Iron Aluminides and Iron-Aluminium-Chromium Alloys. *Mater. Corros.* **1996**, *47*, 685–694. [[CrossRef](#)]
2. Pint, B.A.; Terrani, K.A.; Brady, M.P.; Cheng, T.; Keiser, J.R. High Temperature Oxidation of Fuel Cladding Candidate Materials in Steam–Hydrogen Environments. *J. Nucl. Mater.* **2013**, *440*, 420–427. [[CrossRef](#)]
3. Yamamoto, Y.; Pint, B.A.; Terrani, K.A.; Field, K.G.; Yang, Y.; Snead, L.L. Development and Property Evaluation of Nuclear Grade Wrought FeCrAl Fuel Cladding for Light Water Reactors. *J. Nucl. Mater.* **2015**, *467*, 703–716. [[CrossRef](#)]
4. Field, K.G.; Briggs, S.A.; Sridharan, K.; Howard, R.H.; Yamamoto, Y. Mechanical Properties of Neutron-Irradiated Model and Commercial FeCrAl Alloys. *J. Nucl. Mater.* **2017**, *489*, 118–128. [[CrossRef](#)]
5. Eklund, J.; Hanif, I.; Bigdeli, S.; Jonsson, T. High Temperature Corrosion Behavior of FeCrAlSi Model Alloys in the Presence of Water Vapor and KCl at 600 °C—The Influence of Cr Content. *Corros. Sci.* **2022**, *198*, 110114. [[CrossRef](#)]
6. Sun, Z.; Yamamoto, Y.; Chen, X. Impact Toughness of Commercial and Model FeCrAl Alloys. *Mater. Sci. Eng. A* **2018**, *734*, 93–101. [[CrossRef](#)]

7. Liang, X.; Wang, H.; Pan, Q.; Zheng, J.; Liu, H.; Zhang, R.; Xu, Y.; Xu, Y.; Yi, D. Recrystallization and Mechanical Properties of Cold-Rolled FeCrAl Alloy during Annealing. *J. Iron Steel Res. Int.* **2020**, *27*, 549–565. [[CrossRef](#)]
8. He, B.B.; Hu, B.; Yen, H.W.; Cheng, G.J.; Wang, Z.K.; Luo, H.W.; Huang, M.X. High Dislocation Density-Induced Large Ductility in Deformed and Partitioned Steels. *Science* **2017**, *357*, 1029–1032. [[CrossRef](#)]
9. Sajuri, Z.; Mohamad Selamat, N.F.; Baghdadi, A.H.; Rajabi, A.; Omar, M.Z.; Kokabi, A.H.; Syarif, J. Cold-Rolling Strain Hardening Effect on the Microstructure, Serration-Flow Behaviour and Dislocation Density of Friction Stir Welded AA5083. *Metals* **2020**, *10*, 70. [[CrossRef](#)]
10. Cruise, R.B.; Gardner, L. Residual Stress Analysis of Structural Stainless Steel Sections. *J. Constr. Steel Res.* **2008**, *64*, 352–366. [[CrossRef](#)]
11. Park, S.-J.; Muraishi, S. Micromechanical Analysis of Residual Stress around Coarse Precipitates under Cold Rolling Conditions. *Mech. Mater.* **2021**, *157*, 103841. [[CrossRef](#)]
12. Shi, Y.; Cui, S.; Zhu, T.; Gu, S.; Shen, X. Microstructure and Intergranular Corrosion Behavior of HAZ in DP-TIG Welded DSS Joints. *J. Mater. Process. Technol.* **2018**, *256*, 254–261. [[CrossRef](#)]
13. Gurova, T.; Gomes, L.S.; Peripolli, S.B.; Chavez, G.F.S.; Estefen, S.F.; Leontiev, A. Misorientation Changes and Residual Stresses Redistribution after Welding. A Physical Simulation. *Mater. Res.* **2019**, *22*, e20190360. [[CrossRef](#)]
14. Shrestha, D.; Azarmi, F.; Tangpong, X.W. Effect of Heat Treatment on Residual Stress of Cold Sprayed Nickel-Based Superalloys. *J. Therm. Spray Technol.* **2022**, *31*, 197–205. [[CrossRef](#)]
15. Weng, Z.; Liu, X.; Gu, K.; Guo, J.; Cui, C.; Wang, J. Modification of Residual Stress and Microstructure in Aluminium Alloy by Cryogenic Treatment. *Mater. Sci. Technol.* **2020**, *36*, 1547–1555. [[CrossRef](#)]
16. Shang, F.; Kong, J.; Du, D.; Zhang, Z.; Li, Y. Effect of Cryogenic Treatment on Internal Residual Stresses of Hydrogen-Resistant Steel. *Micromachines* **2021**, *12*, 1179. [[CrossRef](#)] [[PubMed](#)]
17. Huang, X.; Wang, H.; Qiu, S.; Zhang, Y.; He, K.; Wu, B. Cold-Rolling & Annealing Process for Nuclear Grade Wrought FeCrAl Cladding Alloy to Enhance the Strength and Ductility. *J. Mater. Process. Technol.* **2020**, *277*, 116434. [[CrossRef](#)]
18. Mishra, R.S.; De, P.S.; Kumar, N. Residual Stresses and Mitigation Strategies. In *Friction Stir Welding and Processing: Science and Engineering*; Springer International Publishing: Cham, Switzerland, 2014; pp. 297–326, ISBN 978-3-319-07043-8.
19. Zha, X.-Q.; Xiong, Y.; Gao, L.-Q.; Zhang, X.-Y.; Ren, F.-Z.; Wang, G.-X.; Cao, W. Effect of Annealing on Microstructure and Mechanical Properties of Cryo-Rolled 316LN Austenite Stainless Steel. *Mater. Res. Express* **2019**, *6*, 96506. [[CrossRef](#)]
20. Bianchi, I.; Forcellese, A.; Simoncini, M.; Vita, A. Effect of in Situ and Furnace Thermal Annealing on the Mechanical Properties and Sustainability of 3D Printed Carbon-Peek Composites. *Proc. Inst. Mech. Eng. Part B J. Eng. Manuf.* **2023**, *09544054231209797*. [[CrossRef](#)]
21. Pan, L.; He, W.; Gu, B. Effects of Electric Current Pulses on Mechanical Properties and Microstructures of As-Quenched Medium Carbon Steel. *Mater. Sci. Eng. A* **2016**, *662*, 404–411. [[CrossRef](#)]
22. Yi, K.; Xiang, S.; Zhou, M.; Zhang, X.; Du, F. Altering the Residual Stress in High-Carbon Steel through Promoted Dislocation Movement and Accelerated Carbon Diffusion by Pulsed Electric Current. *Acta Metall. Sin. Engl. Lett.* **2023**, *36*, 1511–1522. [[CrossRef](#)]
23. Xiang, S.; Zhang, X. Residual Stress Removal Under Pulsed Electric Current. *Acta Metall. Sin. Engl. Lett.* **2020**, *33*, 281–289. [[CrossRef](#)]
24. Long, P. Influence of Electropulsing Treatment on Residual Stresses and Tensile Strength of As-Quenched Medium Carbon Steel. *J. Phys. Conf. Ser.* **2019**, *1187*, 32054. [[CrossRef](#)]
25. Haque, A.; Sherbondy, J.; Warywoba, D.; Hsu, P.; Roy, S. Room-Temperature Stress Reduction in Welded Joints through Electropulsing. *J. Mater. Process. Technol.* **2022**, *299*, 117391. [[CrossRef](#)]
26. Yamaguchi, A.; Nasu, S.; Tanigawa, H.; Ono, T.; Miyake, K.; Mibu, K.; Shinjo, T. Effect of Joule Heating in Current-Driven Domain Wall Motion. *Appl. Phys. Lett.* **2004**, *86*, 12511. [[CrossRef](#)]
27. Lienig, J.; Thiele, M. *Fundamentals of Electromigration-Aware Integrated Circuit Design*; Springer: Cham, Switzerland, 2018; ISBN 978-3-319-73557-3. [[CrossRef](#)]
28. Mecklenburg, M.; Zutter, B.T.; Ling, X.Y.; Hubbard, W.A.; Regan, B.C. Visualizing the Electron Wind Force in the Elastic Regime. *Nano Lett.* **2021**, *21*, 10172–10177. [[CrossRef](#)] [[PubMed](#)]
29. Sheng, Y.; Hua, Y.; Wang, X.; Zhao, X.; Chen, L.; Zhou, H.; Wang, J.; Berndt, C.C.; Li, W. Application of High-Density Electropulsing to Improve the Performance of Metallic Materials: Mechanisms, Microstructure and Properties. *Materials* **2018**, *11*, 185. [[CrossRef](#)] [[PubMed](#)]
30. Cai, Z.; Huang, X. Residual Stress Reduction by Combined Treatment of Pulsed Magnetic Field and Pulsed Current. *Mater. Sci. Eng. A* **2011**, *528*, 6287–6292. [[CrossRef](#)]
31. Xu, Z.S.; Lai, Z.H.; Chen, Y.X. Effect of Electric Current on the Recrystallization Behavior of Cold Worked α -Ti. *Scr. Metall.* **1988**, *22*, 187–190. [[CrossRef](#)]
32. Wu, C.; Zhou, Y.; Liu, B. Experimental and Simulated Investigation of the Deformation Behavior and Microstructural Evolution of Ti6554 Titanium Alloy during an Electropulsing-Assisted Microtension Process. *Mater. Sci. Eng. A* **2022**, *838*, 142745. [[CrossRef](#)]
33. Waryoba, D.; Islam, Z.; Wang, B.; Haque, A. Low Temperature Annealing of Metals with Electrical Wind Force Effects. *J. Mater. Sci. Technol.* **2019**, *35*, 465–472. [[CrossRef](#)]

34. Hoving, S.J.; Lodder, A.; Sorbello, R.S. Finite-Cluster Description of Electromigration. *Phys. Rev. B Condens. Matter* **1982**, *25*, 6178–6187.
35. Fan, S.; He, B.; Liu, M. Effect of Pulse Current Density on Microstructure of Ti-6Al-4V Alloy by Laser Powder Bed Fusion. *Metals* **2022**, *12*, 81327. [CrossRef]
36. Rahman, M.H.; Oh, H.; Waryoba, D.; Haque, A. Room Temperature Control of Grain Orientation via Directionally Modulated Current Pulses. *Mater. Res. Express* **2023**, *10*, 116521. [CrossRef]
37. Rahman, M.H.; Glavin, N.; Haque, A.; Ren, F.; Pearson, S.J. Effect of High Current Density Pulses on Performance Enhancement of Optoelectronic Devices. *ECS J. Solid State Sci. Technol.* **2024**, *13*, 25003. [CrossRef]
38. Trimby, P.; Anderson, I.; Larsen, K.; Hjelmstad, M.; Thomsen, K.; Mehnert, K. Advanced Classification of Microstructures in EBSD Datasets Using AZtecCrystal. *Microsc. Microanal.* **2020**, *26*, 13410. [CrossRef]
39. Wang, R.; Xu, Z.; Jiang, Y.; Tang, G.; Wan, J.; Chou, K.J.-C.; Li, Q. The Coupling of Thermal and Athermal Effect in High-Density Multiple Pulse Continuous Treatment of AZ31. *Mater. Des.* **2022**, *215*, 110495. [CrossRef]
40. Jarzębska, A.; Maj, Ł.; Bieda, M.; Chulist, R.; Wojtas, D.; Wątroba, M.; Janus, K.; Rogal, Ł.; Sztwiertnia, K. Dynamic Recrystallization and Its Effect on Superior Plasticity of Cold-Rolled Bioabsorbable Zinc-Copper Alloys. *Materials* **2021**, *14*, 3483. [CrossRef]
41. Ding, S.; Khan, S.A.; Yanagimoto, J. Metadynamic Recrystallization Behavior of 5083 Aluminum Alloy under Double-Pass Compression and Stress Relaxation Tests. *Mater. Sci. Eng. A* **2021**, *822*, 141673. [CrossRef]
42. Pan, D.; Wang, Y.; Guo, Q.; Zhang, D.; Xu, X.; Zhao, Y. Grain Refinement of Al–Mg–Si Alloy without Any Mechanical Deformation and Matrix Phase Transformation via Cyclic Electro-Pulsing Treatment. *Mater. Sci. Eng. A* **2021**, *807*, 140916. [CrossRef]
43. Ma, R.; Zhang, X. Refining the Microstructure to Strengthen Casting Titanium Alloy by Electric Pulse. *Mater. Sci. Eng. A* **2022**, *849*, 143519. [CrossRef]
44. Lee, M.; Yu, J.; Bae, M.H.; Won, J.W.; Lee, T. Accelerated Recrystallization Behavior of Commercially Pure Titanium Subjected to an Alternating-Current Electropulse. *J. Mater. Res. Technol.* **2021**, *15*, 5706–5711. [CrossRef]
45. Hou, M.; Li, K.; Li, X.; Zhang, X.; Rui, S.; Wu, Y.; Cai, Z. Effects of Pulsed Magnetic Fields of Different Intensities on Dislocation Density, Residual Stress, and Hardness of Cr4Mo4V Steel. *Crystals* **2020**, *10*, 115. [CrossRef]
46. Li, H.; Hsu, E.; Szpunar, J.; Utsunomiya, H.; Sakai, T. Deformation Mechanism and Texture and Microstructure Evolution during High-Speed Rolling of AZ31B Mg Sheets. *J. Mater. Sci.* **2008**, *43*, 7148–7156. [CrossRef]
47. Lingyan, Z.; Yinghao, C.; Fuqiang, Y. Effect of Cold Working on the Residual Stress around the Notch Front of Stress Corrosion Cracking. *IOP Conf. Ser. Mater. Sci. Eng.* **2018**, *408*, 12007. [CrossRef]
48. Terner, M.; Lee, J.; Marchese, G.; Biamino, S.; Hong, H.U. Electron Backscattered Diffraction to Estimate Residual Stress Levels of a Superalloy Produced by Laser Powder Bed Fusion and Subsequent Heat Treatments. *Materials* **2020**, *13*, 4643. [CrossRef]
49. Krawczyk, B.; Cook, P.; Hobbs, J.; Engelberg, D.L. Corrosion Behavior of Cold Rolled Type 316L Stainless Steel in HCl-Containing Environments. *Corrosion* **2017**, *73*, 1346–1358. [CrossRef]
50. Kamachi Mudali, U.; Shankar, P.; Ningshen, S.; Dayal, R.K.; Khatak, H.S.; Raj, B. On the Pitting Corrosion Resistance of Nitrogen Alloyed Cold Worked Austenitic Stainless Steels. *Corros. Sci.* **2002**, *44*, 2183–2198. [CrossRef]
51. Rahnama, A.; Qin, R. Room Temperature Texturing of Austenite/Ferrite Steel by Electropulsing. *Sci. Rep.* **2017**, *7*, 42732. [CrossRef] [PubMed]
52. Zhao, M.; Schlueter, K.; Wurmshuber, M.; Reitgruber, M.; Kiener, D. Open-Cell Tungsten Nanofoams: Scaling Behavior and Structural Disorder Dependence of Young’s Modulus and Flow Strength. *Mater. Des.* **2021**, *197*, 109187. [CrossRef]

Disclaimer/Publisher’s Note: The statements, opinions and data contained in all publications are solely those of the individual author(s) and contributor(s) and not of MDPI and/or the editor(s). MDPI and/or the editor(s) disclaim responsibility for any injury to people or property resulting from any ideas, methods, instructions or products referred to in the content.